View Online
Dynamic Article Links

Dalton Transactions

Cite this: *Dalton Trans.*, 2011, **40**, 7967

www.rsc.org/dalton

PAPER

Evolution of orientation degree, lattice dynamics and electronic band structure properties in nanocrystalline lanthanum-doped bismuth titanate ferroelectric films by chemical solution deposition

Jinzhong Zhang, Xiangui Chen, Kai Jiang, Yude Shen, Yawei Li, Zhigao Hu* and Junhao Chu

Received 16th March 2011, Accepted 17th May 2011
DOI: 10.1039/c1dt10443h

Ferroelectric lanthanum (La)-substituted bismuth titanate ($Bi_{4-x}La_xTi_3O_{12}$, BLT) nanocrystalline films with the composition range of $0 \le x \le 1$ have been directly deposited on n-type Si (100) substrates by chemical solution deposition. The La substitution effects on the preferred orientation, surface morphology, phonon modes, emission bands and electronic band structures of the BLT films have been investigated by microscopy, Raman scattering, photoluminescence and spectroscopic ellipsometry at room temperature. X-Ray diffraction analysis shows that the films are polycrystalline and exhibit the pure perovskite phase structure. With increasing La composition, the (100)-orientation degree can be enhanced and the root-mean-square roughnesses slightly increase from 6.5 to 8.3 nm. It was found that the Raman-active mode A_{1g}[Bi] at about 59 cm^{-1} is unchanged while the B_{1g} and A_{1g}[Ti] phonon modes at about 648 and 853 cm^{-1} are shifted towards higher frequency by about 36.6 and 8.4 cm^{-1}, respectively. Photoluminescence spectra show that the intensity of the peak located at about 2.3 eV increases with the La composition, except for the $Bi_3LaTi_3O_{12}$ film, due to the smallest grain size and oxygen vacancy defects. The optical constants of the BLT films have been uniquely extracted by fitting the measured ellipsometric spectra with a four-phase layered model (air/surface rough layer/BLT/Si) in the photon energy range of 0.73–4.77 eV. The Adachi dielectric function model has been successfully applied and reasonably describes the optical response behavior of the ferroelectric BLT films. Moreover, the film packing density decreases while the optical band gap linearly increases from 3.610 ± 0.066 to 3.758 ± 0.068 eV with increasing La composition. It is surmised that the phenomena are mainly ascribed to the variations of the electronic structure, especially for the conduction band, which is perturbed by the La doping.

1 Introduction

Ferroelectrics of the bismuth layer perovskite type have received much attention because of their potential applications in the field of microelectronic nonvolatile memories, ferroelectric random-access memories and pyroelectric detectors.[1–4] As we know, bismuth titanate $Bi_4Ti_3O_{12}$ (BIT) belongs to the family of Aurivillius compounds with a general formula of $(Bi_2O_2)(Me_{m-1}R_mO_{3m+1})$, consisting of a fluorite-type sheet $(Bi_2O_2)^{2+}$ interleaved with pseudo-perovskite-type blocks $(Me_{m-1}R_mO_{3m+1})^{2-}$, where Me is mono-, di- or trivalent ions; R is tetra-, penta- or hexavalent ions that enter the pseudo-perovskite unit and m is the number of octahedra RO_6 stacked along the direction perpendicular to the sheets (m = 1, 2, 3, 4, ...).[5] For BIT, Me = Bi, R = Ti, m = 3, and its crystalline structure consists of three $(Bi_2Ti_3O_{10})^{2-}$ blocks sandwiched between two $(Bi_2O_2)^{2+}$ sheets along the tetragonal c axis.[6,7] More importantly, BIT films can be deposited at 650 °C, which is significantly lower than the synthesis temperature of other layer-type ferroelectric materials such as $SrBi_2Ta_2O_9$. In addition, compared with undoped BIT, lanthanum (La)-substituted bismuth titanate ($Bi_{4-x}La_xTi_3O_{12}$, BLT) has the significant advantages in electrical properties such as larger remnant polarization (P_r), smaller coercive field (E_c), lower dielectric loss and higher fatigue resistivity. The electrical properties of the BLT bulk and film materials have been the most extensively studied, while the detailed microstructure and optical properties, which are directly related to electronic band structures, have not been fully clarified.

Recently, optical properties of the pure and La-substituted BIT bulk and films have received much attention in view of their physicochemical properties such as high dielectric constant, excellent electro-optical, photocatalytic activity, low processing temperature and wide band gap. Such materials can be used in potential applications such as dielectrics, electro-optics devices, photocatalysts and ultraviolet detectors.[8–10] However, it should be noted that optoelectronic devices based on ferroelectric materials

Key Laboratory of Polar Materials and Devices, Ministry of Education, East China Normal University, Shanghai, 200241, People's Republic of China. E-mail: zghu@ee.ecnu.edu.cn; Fax: +86-21-54345119; Tel: +86-21-54345150

are still in the preliminary stage owing to incomplete knowledge about the physical parameters related to the applications of integrated optics devices. For example, Yao *et al.* argued that there is photocatalytic activity of BIT powders towards methyl orange as a model organic compound because of the bond angle of Ti–O–Ti and consequent intraelectric field formed between the $(Bi_2O_2)^{2+}$ sheets and the $(Bi_2Ti_3O_{10})^{2-}$ blocks, which are assumed to facilitate the separation of photogenerated electron–hole pairs.[8] In addition, the band gap of the BIT film was evaluated from the ultraviolet–visible absorption spectra to be about 3.08 eV.[8] On the other hand, Hu *et al.* reported that the experimental band gap of a $Bi_{3.25}La_{0.75}Ti_3O_{12}$ film at room temperature was about 3.82 eV, which was derived from transmittance spectra.[9] It has been theoretically reported that the fundamental band gap of the material is indirect, with the conduction band minimum at the Brillouin zone center Γ and the valence band maximum at a zone border, and the theoretical band gap is around 1.2 eV by the local density approximation (LDA), using the parametrization by Perdew and Wang.[6] Recently, Wei *et al.* adopted the generalized gradient approximation (GGA) with the Perdew–Burke–Ernzerhof (PBE) scheme and the calculated values of the direct band gap at the Γ point and the indirect band gap are 1.24 and 0.50 eV (X → Γ), respectively.[11] However, Roy *et al.* argued that the direct and indirect band gaps are 2.30 (Γ → Γ) and 2.17 eV (E → Γ) by using the same method.[12] Therefore, there are some controversies in the optical properties and further investigations are required to explore possible applications in metal-oxide-semiconductor devices and ultraviolet detectors arising from the high dielectric constant and wide band gap.[13]

There are many spectral techniques to extract dielectric functions of films such as transmittance, reflectance and spectroscopic ellipsometry (SE). Among them, SE based on the reflectance configuration is easily adopted for the determination of optical constants.[14] It is a powerful and nondestructive tool, which is sensitive to ultrathin films and surfaces, and allows us to obtain the thickness and optical characteristics of a multi-layer system without the Kramer–Kröning transformation due to determination of two independent physical parameters simultaneously.[15] It is noted that SE can directly provide dielectric constants, optical band gap, absorption coefficient, *etc.* Therefore, this makes it possible to investigate the optical properties of BLT films in a wider photon energy range. In order to explain the distinguishing physical phenomena and further exploit La-substituted BIT materials as a viable candidate for fabricating optoelectronic, capacitor devices and ultraviolet detectors, the La-related optical properties and/or electronic structures should be thoroughly studied and provide a critical reference for device designs and performance optimizations from BLT materials.

In this article, the degree of orientation, surface morphology, phonon modes and optical properties of ferroelectric BLT films with different La compositions have been investigated. The optical constants from the near-infrared to ultraviolet (NIR–UV) photon energy range have been extracted by the SE technique. A dielectric function model related to the interband transition is presented to well reproduce the experimental ellipsometric spectra. Effects of the La composition on the microstructure and electronic band structures of BLT films are discussed in detail.

2 Experimental

2.1 Preparation of the precursor solution

The ferroelectric BLT films were deposited directly on n-type Si(100) substrates by chemical solution deposition employing a spin-coating process. In order to monitor the effects of La composition on the microstructure and optical properties, the $Bi_{4-x}La_xTi_3O_{12}$ films were prepared in the La-substitution range of $0 \le x \le 1$ at 0.25 intervals (*i.e.*, $Bi_4Ti_3O_{12}$, $Bi_{3.75}La_{0.25}Ti_3O_{12}$, $Bi_{3.50}La_{0.50}Ti_3O_{12}$, $Bi_{3.25}La_{0.75}Ti_3O_{12}$ and $Bi_3LaTi_3O_{12}$, or in short, BLT0.00, BLT0.25, BLT0.50, BLT0.75 and BLT1.00, respectively). Analytically pure bismuth nitrate ($Bi(NO_3)_3·5H_2O$, 99.0%), lanthanum nitrate ($La(NO_3)_3·6H_2O$, 98.0%) and titanium butoxide ($Ti[O(CH_2)_3CH_3]_4$, 98.0%) were used as the starting materials. As shown in Scheme 1, the required $Bi(NO_3)_3·5H_2O$ and $La(NO_3)_3·6H_2O$ were mixed in the required molar ratio of Bi and La and then dissolved in a mixture of ethylene glycol monomethyl ether ($C_3H_8O_2$, 99.0%) and heated glacial acetic acid (CH_3COOH, 99.5%) with a volume ratio of 2 : 1; subsequently, an appropriate amount of acetylacetone ($C_5H_8O_2$, 99.0%) was added to stabilize the solution. Note that excess 8 mol% Bi precursor was added for compensating the Bi evaporation during the annealing process. The appropriate amount of $Ti[O(CH_2)_3CH_3]_4$ was also added into the solution, the concentration of which was controlled to 0.06 M for BLT deposition. Finally, all the precursor solutions with different La compositions were stirred for 2.5 h at about 50 °C to improve the homogeneity. The precursor solutions were stabilized for about 40 days before spin coating onto Si substrates to enhance the hydrolysis and polymerization.

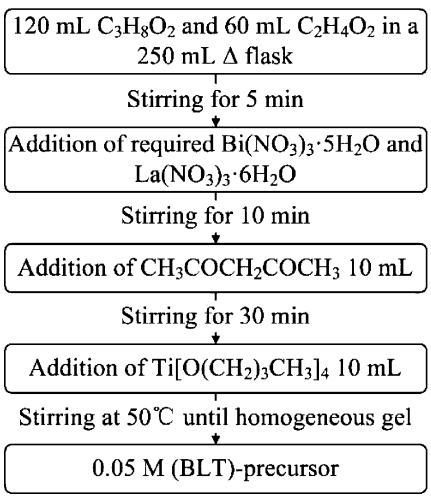

Scheme 1 Preparation process for pure and La-substituted BIT precursors.

2.2 Fabrication of the BLT films

Before the deposition of the BLT films, the n-type Si(100) substrates were cleaned in pure ethanol with an ultrasonic bath to remove physisorbed organic molecules from the surfaces and then the substrates were rinsed repeatedly with deionized water. Finally the substrates were dried in a pure nitrogen stream. The BLT films with different La compositions were deposited by spin coating of the 0.06 M solution onto the Si substrates at a speed of

4000 rpm for 20 s. The as-prepared layers were dried at 180 °C for 200 s, then pyrolyzed at 380 °C for 240 s to remove residual organic compounds, followed by annealing at 700 °C for 240 s in ambient air by a rapid thermal annealing procedure. The average thickness of a single-annealed layer of the BLT films was measured by SE and was found to be about 20 nm. The deposition and annealing-treatment procedures were repeated eight times to obtain the desired thickness.

2.3 XRD, AFM and SEM characterizations

The crystalline structure of the BLT films was investigated by X-ray diffraction (XRD) using a Ni-filtered Cu-Kα radiation source (D/MAX-2550V, Rigaku Co.). In the XRD measurement a vertical goniometer (Model RINT2000) and continuous scanning mode (θ–2θ) were selected with an scanning rate of 10° min^{-1} and interval of 0.02°. The surface morphology of the films was examined by atomic force microscopy (AFM) (Digital Instruments Dimension 3100, Veeco). The scale height is 50 nm and the measured area was $5 \times 5\ \mu m^2$. The grain morphology and thickness were examined by scanning electron microscopy (SEM) (Philips XL30FEG).

2.4 Raman, PL and SE measurements

Raman scattering were recorded by a micro-Raman spectrometer (Jobin-Yvon LabRAM HR 800 UV) and 488 and 325 nm laser lines were applied as the excited sources. Photoluminescence (PL) spectra were measured by the same instrument and the excited source was the 325 nm (3.82 eV) line of a He–Cd laser. The ellipsometric measurements were carried out by a NIR–UV SE in the wavelength range of 260–1700 nm (0.73–4.77 eV) with a spectral resolution of 2 nm (SC630UVN; Shanghai Sanco Instrument, Co., Ltd.). The incident angle was selected to 70° for the films corresponding to the experimental optimization near the Brewster angle of the Si (100) substrates. Note that the films were characterized at room temperature and no mathematical smoothing was performed on the experimental data.

3 Results and discussion

3.1 Microstructure analysis

The XRD patterns of the BLT films with different La compositions annealed at 700 °C are shown in Fig. 1. It can be seen that all the films are polycrystalline with a stronger (117) diffraction peak, whose position (2θ) is located at about 30.1°. Besides the strong feature, there are several other weaker diffraction peaks (006), (200/020), (008), (028/208), *etc.* and no impurity phase is observed, which confirms that the films are of a single perovskite phase. This suggests that the La atoms have been successfully incorporated into the BIT host lattice. It should be pointed out that the *a* and *b* axes could not be distinguished because the crystals are polydomain and $a \approx b$.[16] Based on the (200/020) and (117) diffraction peaks, the lattice constant *a*(*b*) of the La-doped films increases from 5.396 ± 0.008 to 5.402 ± 0.007 Å with the La composition, while the lattice constant *c* decreases from 32.988 ± 0.025 to 32.854 ± 0.021 Å except for the BLT1.00 film, whose value is 32.875 ± 0.028 Å (see Table 1). The deviations of the lattice constant suggest that there are different lattice distortions in the BLT films. Furthermore, the average grain size *r* can be calculated to about 25 nm from the (117) diffraction peak according to the well-known Scherrer equation. It was found that the grain size (about 18 nm) of the BLT1.00 film is the smallest, corresponding to the largest value of the full width at half maximum (FWHM). In addition, the XRD patterns show that the intensities of peaks (00*l*) decrease while those of (*h*00) or (0*k*0) increase with increasing La composition. This illustrates that the BLT films have a certain orientation in *ab*-plane based on the varied intensities. For characterizing the degree of *a*(*b*)- and *c*-axis orientation with the La composition, the magnitudes of the (100) and (001) orientation ($\alpha_{(100)}$ and $\alpha_{(100)}$) are defined as the ratios of intensity of a peak to the sum of intensities of all peaks in the XRD patterns, and the formula can be written as:[17]

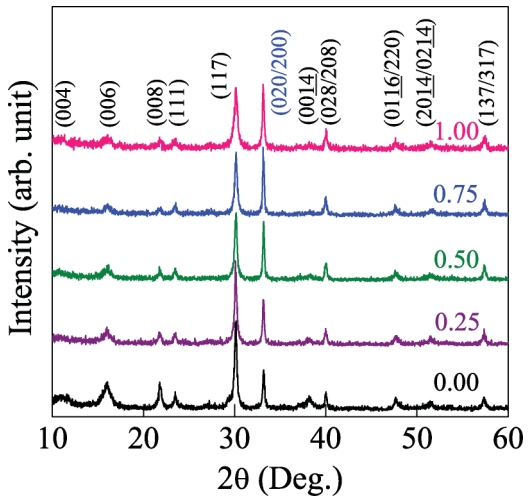

Fig. 1 XRD patterns of the BLT0.00, BLT0.25, BLT0.50, BLT0.75 and BLT1.00 films grown on n-type Si (100) substrates.

Table 1 The position and FWHM of the (117) and (200/020) diffraction peaks for the BLT films determined from the XRD patterns in Fig. 1. The 95% reliability level of the parameters is indicated (±)

	Peak position/°		FWHM/°	Lattice constants		Grain size
Sample	(117)	(200/020)	(117)	*a*(*b*)/Å	*c*/Å	*r*/nm
BLT0.00	30.112 ± 0.006	33.179 ± 0.005	0.275 ± 0.011	5.396 ± 0.008	32.988 ± 0.025	24.8 ± 0.7
BLT0.25	30.112 ± 0.005	33.155 ± 0.004	0.241 ± 0.011	5.398 ± 0.006	32.944 ± 0.019	26.9 ± 0.8
BLT0.50	30.129 ± 0.005	33.177 ± 0.003	0.226 ± 0.010	5.398 ± 0.005	32.939 ± 0.018	25.1 ± 0.7
BLT0.75	30.148 ± 0.006	33.155 ± 0.003	0.235 ± 0.012	5.399 ± 0.005	32.854 ± 0.021	23.0 ± 0.7
BLT1.00	30.134 ± 0.008	33.143 ± 0.004	0.266 ± 0.017	5.402 ± 0.007	32.875 ± 0.028	18.0 ± 0.6

$$\alpha_{(100)} = \frac{I_{(200/020)}}{\sum_{\text{all peaks}} I_{(hkl)}}, \quad \alpha_{(001)} = \frac{I_{(006)}}{\sum_{\text{all peaks}} I_{(hkl)}} \qquad (1)$$

where $I_{(200)/(020)}$, $I_{(006)}$ and $\sum_{\text{all peaks}} I_{(hkl)}$ are the intensities of the peaks (200)/(020), (006) and the sum of intensities of all peaks in the XRD patterns, respectively. Fig. 2a and b show the changes and relative variations of the *a*- and *c*-orientation degree with increasing La composition, respectively, and suggest that the La-substitution enhances the degree of *a*-orientation, in which direction the spontaneous polarization is much larger than that in the *c*-direction at room temperature.[18] In addition, the grain size can play an important role in the preferred orientation since the smallest grain size of the BLT1.00 film decreases the degree of the *a*-orientation.

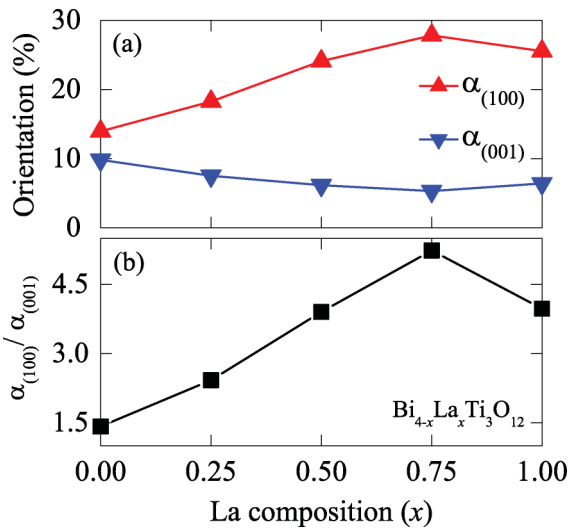

Fig. 2 (a) La-composition dependence of the degree for the *a*(*b*)- and *c*-preferred orientation, $\alpha_{(100)}$ and $\alpha_{(001)}$; (b) the ratio of the $\alpha_{(100)}$- and $\alpha_{(001)}$-orientation of the BLT films.

3.2 Morphology patterns

Fig. 3 shows three-dimensional AFM images of the BLT films. The images suggest that the surface morphology presents a similar pattern, while the root-mean-square roughness is estimated to 6.5, 7.3, 7.3, 7.5 and 8.3 nm for x = 0, 0.25, 0.50, 0.75 and 1, which means that the film surface becomes slightly rougher with increasing La composition. As an example, the plane-view and cross-sectional microstructure of the BLT0.00 and BLT0.50 films are shown in Fig. 4a–d, respectively. The result derived from the AFM images are consistent with those from the SEM images. From the cross-sectional structure, the films have a fluctuating surface and there is a distinct interface between the film and Si substrate; the thickness of the BLT films is about 160 ± 10 nm. Owing to the identical growth conditions, the BLT films present similar morphology with the La replacement, indicating that the films are highly homogenous. Therefore, the variations of grain size and surface morphology can affect the lattice vibrations and optical properties of the films discussed in the following.

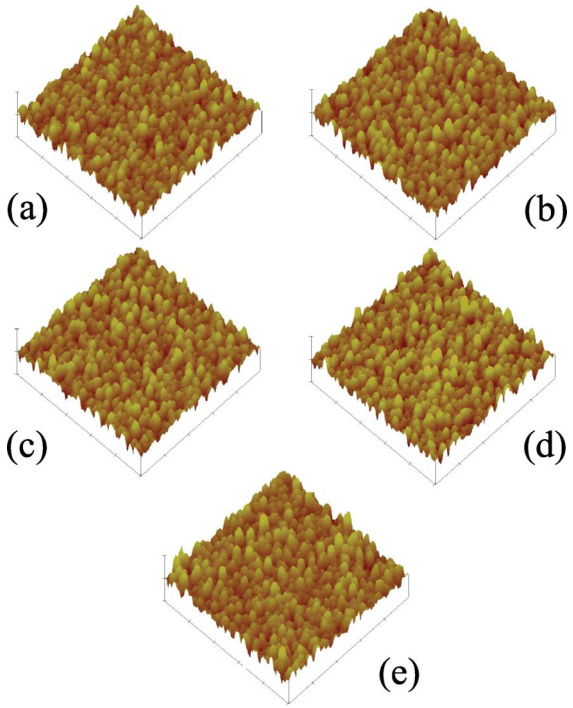

Fig. 3 The AFM three-dimensional images of (a) BLT0.00, (b) BLT0.25, (c) BLT0.50, (d) BLT0.75 and (e) BLT1.00, respectively. Note that the scale height is 50 nm and the measured area is 5 × 5 μm², respectively.

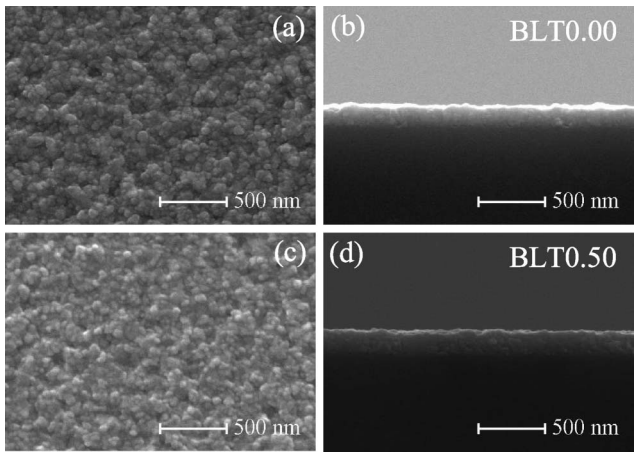

Fig. 4 Plane-view and cross-sectional SEM images of the BLT films on n-type Si (100) substrates: (top) BLT0.00 film, (bottom) BLT0.50 film.

3.3 Lattice dynamics

For ferroelectric BIT single crystals, there are two suggested models at room temperature, a monoclinic system with space group *B*1*a*1 and an orthorhombic system with space group *B*2*cb*.[19,20] Recently, it has been found that the changes of symmetry are *B*1*a*1 → *B*2*cb* → *F*2*mm* → *I*4/*mmm* as the temperature increases and that *B*2*cb* and *F*2*mm* are two intermediate phases.[21,22] This means that the monoclinic system *B*1*a*1 is more suitable than the orthorhombic one *B*2*cb* as a crystal structural system of BIT or BLT materials at room temperature even though both of them are commensurate modulations of the nonpolar orthorhombic parent *Fmmm*. The parent structure *Fmmm* is predicted to have

24 first-order Raman-active modes ($6A_g + 2B_{1g} + 8B_{2g} + 8B_{3g}$), two inactive modes ($2A_u$) and 28 infrared-active modes ($8B_{1u} + 10B_{2u} + 10B_{3u}$) at the Γ point of the Brillouin zone (*i.e.*, $q = 0$).[2,23] Fig. 5a and b show the Raman-active phonon modes of the BLT films with the laser lines of 488 and 325 nm, respectively. Only twelve Raman modes of the films and one mode of the Si substrate are observed in the wavenumber range from 50 to 1000 cm^{-1}, which can be attributed to the overlap of the same symmetry vibrations or the weak features of some vibration bands. Up to now, the assignments of the Raman modes are still not clear for BLT materials, because of their complex crystal structure. It has been reported that the Raman modes at about 155, 273 and 853 cm^{-1} can be assigned as A_{1g} phonon modes and those at about 228 and 648 cm^{-1} are the B_{2g}/B_{3g} and B_{1g} phonons, respectively.[2,24] In addition, the modes above 200 cm^{-1} are related to the TiO_6 octahedra, which is due to the large intragroup binding energy in the TiO_6 and small mass of Ti^{4+} ions. The triple bands at around 83, 120 and 155 cm^{-1} originate from the displacement of the Bi^{3+} ions in the perovskite blocks.[25] As seen in Fig. 5a, the intensities of the mode located at 120 cm^{-1} decreases while that of the mode at about 155 cm^{-1} increases with increasing La composition, which means that the La^{3+} ions substitute the Bi^{3+} ions in the perovskite units.

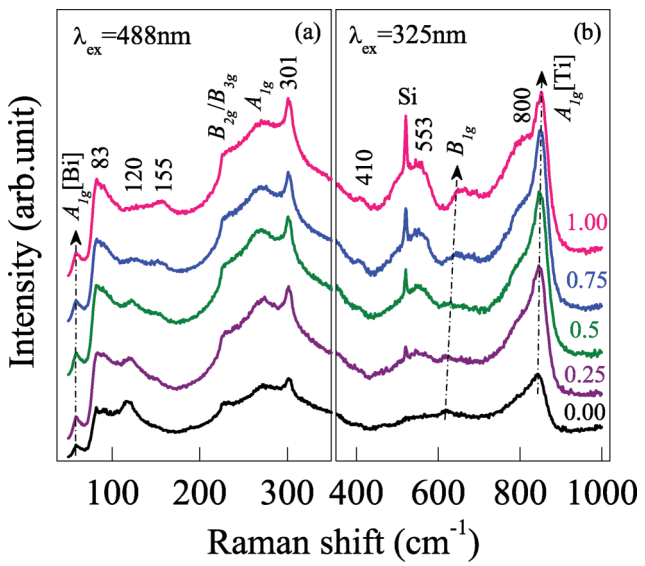

Fig. 5 Raman spectra of the BLT films under excitation lines of (a) 488 and (b) 325 nm, respectively. The arrows show the variation trend of the Raman-active phonon frequencies at about 59, 648 and 853 cm^{-1}, respectively.

Based on the microstructure of the layer-type compound, three types of La substitutions for Bi atoms in BLT are reasonable: La atoms can substitute for Bi atoms in the $(Bi_2O_2)^{2+}$ sheets only, in the $(Bi_2Ti_3O_{10})^{2-}$ blocks only, or in both. In order to determine the location of La atoms in the present BLT films, the La composition dependence of the frequencies for Raman-active modes A_{1g}[Bi], B_{2g} and A_{1g}[Ti] at about 59, 648 and 853 cm^{-1} are shown in Fig. 6a–c, respectively. The composition dependence of the Raman-active modes can be well expressed by $(59.1 - 0.3x)$, $(613.3 + 36.6x)$ and $(843.2 + 8.4x)$ cm^{-1}, respectively. It suggests that the Raman phonon frequency of A_{1g}[Bi] does not change while those of the other two are shifted towards higher frequency by about 36.6 and 8.4 cm^{-1} (for $x = 1$), respectively. The A_{1g}[Bi] mode as a

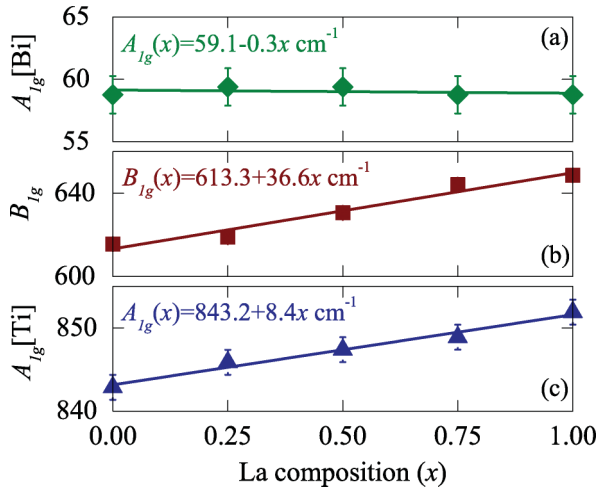

Fig. 6 The La composition dependence of (a) A_{1g}[Bi], (b) B_{1g} and (c) A_{1g}[Ti] phonon modes for the BLT films. The solid lines are the linearly fitted results as a guide for the eye.

"rigid layer" mode originated from the Bi–O bonds of the $(Bi_2O_2)^{2+}$ sheets against the perovskite units. If the Bi^{3+} ions in the sheets are replaced by the La^{3+} ions, the mode may show a red shift because the mass of La^{3+} is smaller than that of Bi^{3+}. Therefore, La atoms mainly substitute for Bi atoms in the perovskite units of the BLT films. The mode A_{1g}[Ti] is assigned to the stretching mode of TiO_6. The fact that the varied upshifts of the modes at about 648 and 853 cm^{-1} are related to the vibrations of the TiO_6 octahedra confirms the above viewpoint because of the La replacement in the perovskite units. Note that the Bi^{3+} and/or La^{3+} orbital hybridization with the O_{2p} orbital ions can strengthen the short-range repulsion, which leads to less octahedral distortion.[26,27]

3.4 PL emissions

PL is a nondestructive and high-sensitivity tool, which is widely adopted to study the photochemistry and photophysics of dielectric and semiconductor materials in the photocatalysis field. In addition, PL can supply information such as lattice defects, grain boundary and surface/subsurface oxygen vacancies, as well as the separation and recombination of photoinduced charge carriers.[28,29] Theoretically the interaction between Bi and O atoms can be in favor of the generation and separation of the photoexcited electron–hole pairs in the BIT material.[11] Fig. 7 shows the room-temperature PL emission spectra of the ferroelectric BLT films with different La compositions. There are two visible broad peaks between 1.5 and 3.0 eV (410–830 nm) with the maximum intensity at about 2.3 eV. Note that the intensity and position of the broad structure located at about 2.9 eV remains unchanged with the La composition and may originate from the instrument system and/or background, whose signal has been collected separately. It is found that the peak position at about 2.3 eV in the PL spectra has a small blue shift as a function of the La composition, as shown in the inset of Fig. 7, and its intensity is quite sensitive to the La-doping composition. The emission intensities at about 2.3 eV for the BLT films increase with increasing La composition except for that of the BLT1.00 sample, due to the smallest grain size, which could capture more photoinduced electrons and reduce their recombination with photoinduced holes at the grain boundaries.[30]

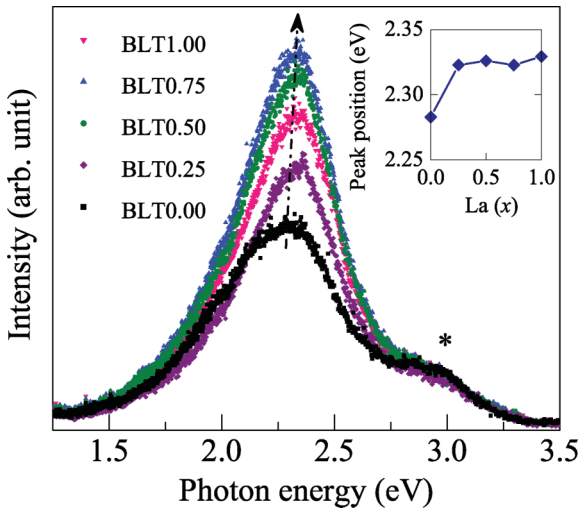

Fig. 7 Composition dependence of room-temperature PL emission spectra from the BLT films. The arrow shows the upshift of the peak position located at about 2.3 eV. The inset indicates the varied peak position with the La composition.

Since the grain size of the BLT films is of similar values (25 nm) except for that of the BLT100 sample (18 nm), the effect of the grain size on the PL intensity is less significant as compared to the doping behavior. On the other hand, it has been reported that the grain size may induce a blueshift of the luminescence peak position.[31] It can be used to explain the phenomena illustrated in the inset of Fig. 7, where the PL photon energy approached the maximum value for the BLT1.00 sample, with the smallest grain size.

Generally, the PL efficiency η_R can be calculated by the formula given in eqn (2):[32]

$$\eta_R \equiv \frac{(dN/dt)_{radiative}}{(dN/dt)_{total}} = \frac{1}{1+\tau_R/\tau_{NR}} \quad (2)$$

where N is the number of photons emitted in a given time t, τ_R and τ_{NR} is the radiative and non-radiative lifetime of the transition from excited state to ground state. It indicates that if $\tau_R \gg \tau_{NR}$ then η_R is very small ($\eta_R \to 0$) and the light emission is very inefficient. On the other hand, if $\tau_R \ll \tau_{NR}$ then η_R approaches unity ($\eta_R \to 1$) and the maximum possible amount of light is emitted. Thus it is required for efficient luminescence that the radiative lifetime should be much shorter than the non-radiative lifetime. It was reported that defect states such as oxygen vacancies in some ferroelectric and semiconductor oxides also capture electrons, generating a broad green peak.[33] Therefore, the intensities increase with the La composition because the introduction of La could shorten the radiative lifetime by generating more luminescent centers and surface/subsurface oxygen vacancies related to the structure disorder in the BLT films.

3.5 SE theoretical consideration

Based on the reflectance configuration, SE provides an effective tool to extract simultaneously thickness and optical constants of a multilayer system.[14,34,35] It is a nondestructive and high-sensitive optical method that records the relative changes in the amplitude and phase of particular directions polarized light upon oblique reflection from the film surface. The experimental parameters measured by ellipsometry are the angles $\Psi(E)$ and $\Delta(E)$, which are related to the microstructure and optical properties of materials.[15] It should be emphasized that the $\Psi(E)$ and $\Delta(E)$ are the function of incident angle, photon energy, film thickness and optical constants $[\tilde{N}(E) = n(E) + i\kappa(E)]$, *i.e.*, the refractive index $n(E)$ and extinction coefficient $\kappa(E)$ from the system studied. The thickness d_f, optical constants and other basic physical parameters of the film material, such as optical band gap E_g, high-frequency dielectric constant ε_∞ could be extracted from the best fit between the experimental and theoretical spectra.

In order to extract the dielectric functions $[\tilde{\varepsilon}(E) = \varepsilon_r(E) + i\varepsilon_i(E)]$ and other physical parameters of the ferroelectric BLT films on the n-type Si (100) substrates, the SE spectra were studied by a multi-layer model with a four-phase layered structure (*i.e.*, air/surface rough layer/BLT/Si). It should be emphasized that the reliability of the fitting method mainly depends on the selection of the dielectric function models. As we know, Lorentz and Cauchy models are suitable for the transparent region below the band gap of the semiconductor materials. Fortunately, the dielectric functions $\tilde{\varepsilon}(E)$ at photon energies below and above the optical band gap can be calculated by the Adachi's model, which is based on the Kramer–Kröning transformation and is strongly connected with the electronic band structure of materials. The method reveals the distinct structures at the energy of the three-dimensional M_0-type critical point E_g, which is written as:

$$\tilde{\varepsilon}(E) = \varepsilon_\infty + \frac{A_0(2\sqrt{E_g} - \sqrt{E_g + E + i\Gamma} - \sqrt{E_g - E - i\Gamma})}{(E + i\Gamma)^2} \quad (3)$$

Here, ε_∞ is the high-frequency dielectric constant, A_0 and Γ are the strength and broadening values of the optical band gap E_g transition, respectively.[36] Correspondingly, the optical constants $\tilde{N}(E)$ and optical conductivity $\tilde{\sigma}$ can be calculated from the well-known relationships $\tilde{N}(E) = \sqrt{\tilde{\varepsilon}(E)}$ and $\tilde{\sigma}(\omega) \equiv \sigma_r(\omega) + i\sigma_i(\omega) = \varepsilon_0\varepsilon_i\omega + i\varepsilon_0(\varepsilon_r - 1)\omega$, respectively. Here ε_0 and ω are the vacuum dielectric constant and the light frequency, respectively. According to the surface roughnesses of the BLT films detected by the AFM and SEM images, the Brüggeman effective medium approximation (BEMA) was employed to calculate the dielectric function of the rough surface layer.[37] The refractive index of the void component is taken to be unity, the extinction coefficient of void component is zero and the dielectric functions of n-type Si (100) in the fitting process can be directly taken from ref. 38. The best-fit parameter values in eqn (3) can be obtained by the Levenberg–Marquardt algorithm in the linear least-squares curve fitting.[39] The root-mean-square fractional error function has been used to judge the simulated quality between the experimental and calculated data.

3.6 Ellipsometric spectra

As an example, the experimental $\Psi(E)$ and $\Delta(E)$ spectra recorded at the incident angle of 70° for the BLT0.50 and BLT0.75 films on n-type Si (100) substrates are shown by the dotted lines in Fig. 8a and b, respectively. The Fabry–Pérot interference patterns observed in the transparent region below the photon energy of about 3.6 eV, which is due to the multi-reflectance between the film and Si substrate. The dielectric functions of the BLT films can be extracted by fitting the Adachi model to the experimental data. The fitted ellipsometric spectra of the two samples are shown

Table 2 The parameter values of the Adachi dielectric function model for the BLT films determined from the simulation of ellipsometric spectra in Fig. 8. The 95% reliability of the fitting parameters is given with (±)

Sample	ε_∞	A_0/eV$^{3/2}$	E_g/eV	Γ/eV	f_s (%)	d_s/nm	d_f/nm
BLT0.00	1.608 ± 0.029	124.3 ± 2.3	3.610 ± 0.066	0.021 ± 0.004	16.1 ± 0.3	1.9 ± 0.4	152.0 ± 3.0
BLT0.25	1.620 ± 0.029	118.9 ± 2.1	3.647 ± 0.065	0.042 ± 0.008	22.3 ± 0.4	2.8 ± 0.5	152.5 ± 2.7
BLT0.50	1.733 ± 0.030	113.8 ± 1.9	3.679 ± 0.064	0.047 ± 0.008	28.5 ± 0.5	2.8 ± 0.5	155.4 ± 2.7
BLT0.75	1.729 ± 0.032	112.5 ± 2.1	3.703 ± 0.068	0.051 ± 0.009	31.3 ± 0.6	3.2 ± 0.6	156.6 ± 2.9
BLT1.00	1.808 ± 0.033	106.9 ± 1.9	3.758 ± 0.068	0.032 ± 0.006	48.4 ± 0.9	4.2 ± 0.8	158.4 ± 2.9

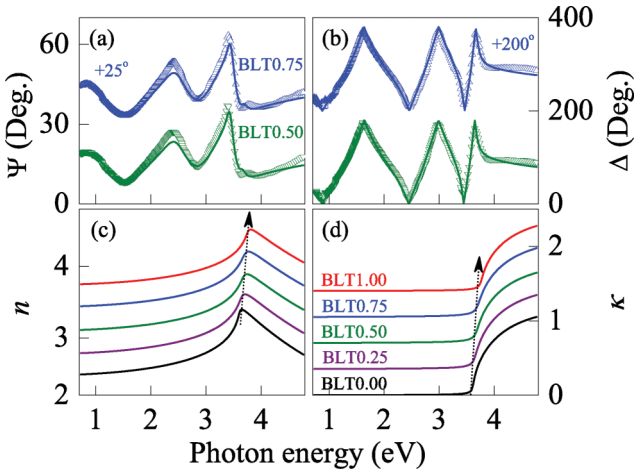

Fig. 8 The near infrared–ultraviolet experimental (dotted lines) and best-fitted ellipsometric (solid lines) spectra (a) $\Psi(E)$ and (b) $\Delta(E)$ of the BLT0.50 and BLT0.75 films. Evolution of (c) refractive index n and (d) extinction coefficient of the BLT films in the phonon energy range from 0.73 to 4.77 eV. For clarity, the arrows indicate the absorption edge blueshift with the La composition. Note that the n and κ are shifted by 0.35.

by the solid lines in Fig. 8a and b, respectively. The values of the parameters in eqn (3), the BLT component f_s and thicknesses of surface rough layer d_s and the thickness of films d_f are summarized in Table 2. Note that the 95% confidence limits for all fitting parameters is given with (±). As can be seen, a good agreement is obtained between the fitted and experimental spectra in the entire measured photon energy range from 0.73 to 4.77 eV. Therefore, it confirms that the dielectric function model used in the present work is reasonable to describe the optical dispersion behavior of the ferroelectric BLT films. From Table 2, the high-frequency dielectric constant, optical band gap, surface roughness layer thickness and film thickness are slightly varied by the La doping in the present films. The variation trend of the surface roughness with the La composition agrees with the results from the AFM images. The total thickness of the BLT films is estimated to be about 154, 156, 156, 160 and 162 nm with increasing x, which also are similar to the data derived from the SEM images. It indicates that the selected Adachi dielectric function model and the four-phase structure can be reasonable and acceptable for the BLT films.

3.7 Optical constants and electronic band structure

The refractive index n and extinction coefficient κ of the BLT films are shown in Fig. 8c and d, respectively. The optical constants variation with the photon energy is the typical optical response behavior of dielectric and/or semiconductor materials.[15,38] Generally, with increasing photon energy, the refractive index increases and approaches the maximum at about 3.65 eV, and then decreases due to the well-known Van Hove singularities.[14] At the photon energy of 2 eV, n increases from 2.42 to 2.58 and the corresponding dielectric constant ε_r is in the range of 5.86–6.66 with decreasing La composition, which is slightly larger than the theoretical value of about 5.6.[40] It was argued that the higher n arises from a low-frequency phonon mode and large Born effective charges.[41] In the transparent region ($E < E_g$), the extinction coefficient is closer to zero and then remarkably increases as the photon energy further increases beyond the fundamental band gap. It suggests that a strong optical absorption appears, which shows the interband electronic transition from the top of the valence band to the bottom of the conduction band for the BLT films. Obviously, the absorption edge is shifted towards a higher photon energy side with increasing La composition, which is illustrated by the arrow. In addition, Fig. 9 shows the optical conductivity of the BLT films with the maximum value of 3000–4000 Ω^{-1} cm^{-1} above 4.5 eV, which is slightly smaller than the calculated value (4500–5500 Ω^{-1} cm^{-1}).[40] Correspondingly, the optical conductivity presents a similar dependence on the photon energy. The slight discrepancy can be ascribed to the polycrystalline structure of the present BLT films grown by the sol–gel technique. On the other hand, the grain boundaries and domain wall can affect the photon-induced carrier transport and further result in less/decreasing conductivity.[42] As compared to the theoretical calculations, both shape and absolute magnitude of the experimental optical conductivity indicate that

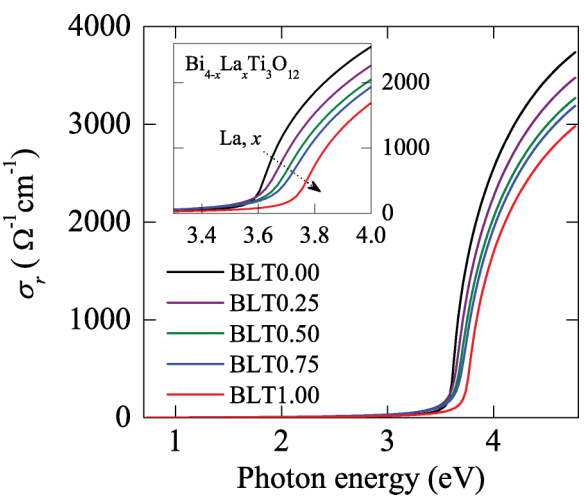

Fig. 9 Real part of the optical conductivity for the BLT films with the La composition in the photon energy range of 0.73–4.77 eV. The inset is the enlarged part around the absorption edge.

the BLT films are of high quality and can be applied to the ultraviolet optoelectronic devices, such as detectors.

Moreover, the refractive index linearly decreases with the La composition in the visible region. The phenomenon can be caused by the decreasing strength of the E_g transition. In addition, it is well known that the refractive index is strongly related to the packing density ρ of a given material by the following Lorentz–Lorentz relation:[43]

$$\frac{n(E)^2-1}{n(E)^2+1}=\frac{4\pi}{3}\frac{N_A}{3}\rho\alpha_m \quad (4)$$

Here N_A is the Avogadro's constant, m is the molecular weight, and α_m is the polarizability. The decrease of n at 2.0 eV could be caused by the lower packing density from eqn (4). Therefore, the La substitution could decrease the packing density of the BLT films. Fig. 10a shows the normalized packing density (ρ) as a function of the La composition at a phonon energy of 2.0 eV. The changing trend can be well expressed by the linear relationship as $1.00 - 0.05x$. The La dependence of the ε_∞ for the BLT films is shown in Fig. 10b. It suggests that the ε_∞ increases with the La composition and it can be expressed by $1.60 + 0.20x$. The high-frequency dielectric constant accounts for the so-called high-frequency limit. Results indicated that the contributions from the high-energy interband transitions become more prominent with the La composition. The Adachi model parameter E_g and its fitted value are shown in Fig. 10c by the dotted and solid lines, respectively, and suggests that the optical band gap increases with the La composition and could be described by the linear relationship $3.61 + 0.14x$. The E_g of the BLT films increases from 3.61 to 3.76 eV, which agrees with that (3.82 eV) reported.[9] For the case of $x = 3$, the Bi atoms in the perovskite units are completely substituted by the La atoms, the band gap of which can be estimated to about 4.03 eV. Note that the value is very close to that (4 eV) of $LaTiO_3$.[44] Therefore, the linear relationship ($3.61 + 0.14x$) could be reasonably effective for the La composition (x) reaching 3, which is much larger than that ($0 \le x \le 1$) investigated in the present work. The result further confirms that the La atom indeed replaces the Bi site of the host matrix. It should be emphasized that the values are much larger than that derived by the theoretical calculation due to the well-known shortcomings of exchange-correction function in describing excited states from the density functional theory calculation.

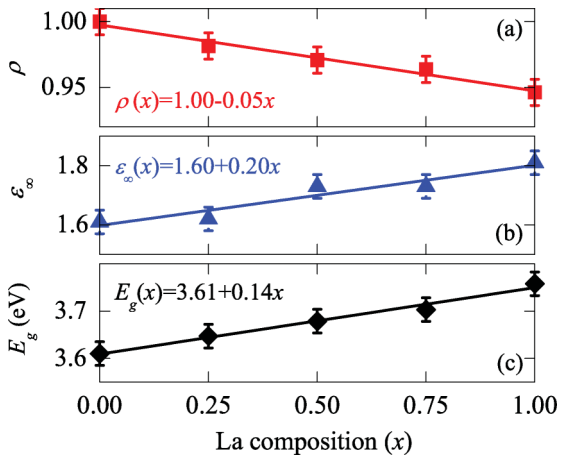

Fig. 10 Composition dependence of (a) the normalized packing density at the phonon energy of 2 eV, (b) high-frequency dielectric constant and (c) optical band gap of the BLT films. The solid lines represent the linearly fitted results.

Recently, it has been reported that the band gap of the pure and La-substituted BIT material is indirect with a value of 2.9 eV and an onset of direct optical transitions at 3.1 eV by using the GGA of the Tran-Blaha and Becke-Johnson (TB–BJ) functional.[40,45,46] It should be noted that the calculated band gap is much smaller than the experimental value (3.61 eV). Unfortunately, there have been few reports on the electronic band structure of the BLT films even though the electronic properties of BIT material are derived by the GGA+U or the quasiparticle self-consistent GW approximations (G is Green's function and W is the screened Coulomb interaction), which is suitable for strongly correlated systems associated with the *e*–*e* interactions. Thus, the band gap calculated for the ferroelectric system could be reasonably enlarged and accepted, as compared to other calculation techniques.[47] As we know, the valance band mainly consists of the O_{2p}, $Bi_{6s,6p}$ and Ti_{3d} states in the perovskite type unit and the O_{2p} orbital is strongly hybridized with the Ti_{3d} (O_{2p}–Ti_{3d}) and Bi (O_{2p}–$Bi_{6s,6p}$) orbital below the Fermi level E_F. However, the conduction band is dominated by the Ti_{3d} states with minor contributions from the Bi_{6p} and O_{2p} states. Also, there is considerable hybridization between Ti_{3d}, Bi_{6p} and O_{2p} in the conduction band.[11,27,48] In the case of La-substituted BIT films, the La atoms substitute the partial Bi atoms in the pseudo-perovskite unit. The E_g of the films increases with the La composition because the La^{3+} ions have no outer electron and only a lone pair of 6s electrons, which reduce the hybridization with the O_{2p} states, in contrast to a Bi^{3+} ion. Therefore, the La substitution should lead to less structural distortion. It should be emphasized that the shift of the E_g to higher energy can not relate to the Burstein–Moss effect because the La^{3+} and Bi^{3+} ions have the same valence of +3 and the substitution La atoms can not contribute electrons or holes. From the viewpoint of BLT-based capacitor devices and UV detectors, a wider optical band gap favors the improvement of its properties, such as decreased leakage current.

4 Conclusion

To summarize, high-quality La-substituted BIT ($0 \le x \le 1$) films have been directly deposited on n-type Si(100) substrates by chemical solution deposition employing a spin-coating process. The XRD analysis shows that the films are polycrystalline and exhibit the pure perovskite phase structure and the substitution of La enhances the (100)-orientation degree from 14 to 28%. The behaviors of the Raman-active modes A_{1g}[Bi], B_{2g} and A_{1g}[Ti] located at about 59, 648 and 853 cm^{-1} illustrate that La atoms substitute the Bi atoms in the perovskite units. With increasing La composition, the intensity of the peak at about 2.3 eV in the PL emission spectra increases, except for the BLT1.00 film due to the smallest grain size. According to the varied intensities of the peak located at about 2.3 eV in the PL spectra, the introduction of La could shorten the radiative lifetime and/or prolong the non-radiative lifetime. Moreover, the dielectric functions of the BLT films has been uniquely extracted by fitting the measured ellipsometric data with the Adachi and four-phase layered models. The refractive index linearly decreases while the high-frequency dielectric constant linearly increases with increasing La

composition due to the decreased packing density. In the BLT films, the La substitution is considered to be one of the most important factors to affect microstructure, lattice vibration and optical properties. The present results could be crucial for future applications of BLT-based optoelectronic devices and UV detectors.

Acknowledgements

One of the authors (Jinzhong Zhang) is grateful to Professors Xiaodong Tang, Wenfei Xu, Wenlei Yu and Zhihua Duan for technical support. This work is financially supported by the Natural Science Foundation of China (Grant Nos. 60906046 and 11074076), Major State Basic Research Development Program of China (Grant Nos. 2007CB924901 and 2011CB922200), Program of New Century Excellent Talents, MOE (Grant No. NCET-08-0192) and PCSIRT, Projects of Science and Technology Commission of Shanghai Municipality (Grant Nos. 10DJ1400201, 10SG28, 10ZR1409800 and 09ZZ42) and The Program for Professor of Special Appointment (Eastern Scholar) at Shanghai Institutions of Higher Learning.

Notes and references

1 H. N. Lee, D. Hesse, N. Zakharov and U. Gosele, *Science*, 2002, **296**, 2006–2009.
2 K. Liang, Y. Qi and C. Lu, *J. Raman Spectrosc.*, 2009, **40**, 2088–2091.
3 Z. Shen, J. Liu, J. Grins, M. Nygren, P. Wang, Y. Kan, H. Yan and U. Sutter, *Adv. Mater.*, 2005, **17**, 676–680.
4 X. F. Ruan, Y. X. Li, X. S. Wang and X. Yao, *Ferroelectrics*, 2010, **404**, 119–126.
5 B. Aurivillius, *Ark. Kemi.*, 1949, **1**, 463–480; B. Aurivillius, *Ark. Kemi.*, 1949, **1**, 499–512; B. Aurivillius, *Ark. Kemi.*, 1950, **2**, 519–527.
6 R. Machado, M. G. Stachiotti, R. L. Migoni and A. H. Tera, *Phys. Rev. B: Condens. Matter Mater. Phys.*, 2004, **70**, 214112.
7 M. W. Chu, M. T. Caldes, L. Brohan, M. Ganne, Marie, O. Joubert and Y. Piffard, *Chem. Mater.*, 2004, **16**, 31–42.
8 W. F. Yao, X. H. Xu, H. Wang, J. T. Zhou, X. N. Yang, Y. Zhang, S. X. Shang and B. B. Huang, *Appl. Catal., B*, 2004, **52**, 109–116.
9 Z. G. Hu, Y. W. Li, F. Y. Yue, Z. Q. Zhu and J. H. Chu, *Appl. Phys. Lett.*, 2007, **91**, 221903.
10 C. Jia, Y. Chen and W. F. Zhang, *J. Appl. Phys.*, 2009, **105**, 113108.
11 W. Wei, Y. Dai and B. B. Huang, *J. Phys. Chem. C*, 2009, **113**, 5658–5663.
12 A. Roy, R. Prasad, S. Auluck and A. Garg, *J. Phys.: Condens. Matter*, 2010, **22**, 165902.
13 Y. Hou, T. Lin, Z. M. Huang, G. S. Wang, Z. G. Hu, J. H. Chu, X. H. Xu and M. Wang, *Appl. Phys. Lett.*, 2004, **85**, 1214–1216.
14 J. Z. Zhang, Y. D. Shen, Y. W. Li, Z. G. Hu and J. H. Chu, *J. Phys. Chem. C*, 2010, **114**, 15157–15164.
15 R. M. A. Azzam, N. M. Bashara, *Eillipsometry and Polarized Light*, North-Holland, Amsterdam, The Netherlands, 1977.
16 D. Nuzhnyy, S. Kamba, P. Kužel, S. Veljko, V. Bovtun, M. Savinov, J. Petzelt, H. Amorín, M. E. V. Costa, A. L. Kholkin, P. Boullay and M. Adamczyk, *Phys. Rev. B: Condens. Matter Mater. Phys.*, 2006, **74**, 134105.
17 J. Müller, J. Nowoczin and H. Schmitt, *Thin Solid Films*, 2006, **496**, 364–370.
18 H. Irie, M. Miyayama and T. Kudo, *J. Appl. Phys.*, 2001, **90**, 4089–4094.
19 A. D. Rae, J. G. Thompson, R. L. Withers and A. C. Willis, *Acta Crystallogr., Sect. B: Struct. Sci.*, 1990, **46**, 474–487.
20 A. Shrinagar, A. Garg, R. Prasad and S. Auluck, *Acta Crystallogr., Sect. A: Found. Crystallogr.*, 2008, **64**, 368–375.
21 J. M. Perez-Mato, P. Blaha, K. Schwarz, M. Aroyo, D. Orobengoa, I. Etxebarria and A. García, *Phys. Rev. B: Condens. Matter Mater. Phys.*, 2008, **77**, 184104.
22 M. K. Jeon, Y. I. Kim, S. H. Nahm and S. I. Woo, *J. Phys. Chem. B*, 2005, **109**, 968–972.
23 H. Idink, V. Srikanth, W. B. White and E. C. Subbarao, *J. Appl. Phys.*, 1994, **76**, 1819–1823.
24 P. R. Graves, G. Hua, S. Myhra and J. G. Thompson, *J. Solid State Chem.*, 1995, **114**, 112–122.
25 M. K. Jeon, Y.-I. Kim, S.-H. Nahm and S. I. Woo, *J. Phys. D: Appl. Phys.*, 2006, **39**, 5080–5085.
26 C. Y. Yau, R. Palan, K. Tran and R. C. Buchanan, *Appl. Phys. Lett.*, 2005, **86**, 032907.
27 Y. Shimakawa, Y. Kubo, Y. Tauchi, H. Asano, T. Kamiyama, F. Izumi and Z. Hiroi, *Appl. Phys. Lett.*, 2001, **79**, 2791–2793.
28 A. Bera, T. Ghosh and D. Basak, *ACS Appl. Mater. Interfaces*, 2010, **2**, 2898–2903.
29 G. S. Armatas and M. G. Kanatzidis, *Nano Lett.*, 2010, **10**, 3330–3336.
30 A. Roldaán, M. Boronat, A. Corma and F. Illas, *J. Phys. Chem. C*, 2010, **114**, 6511–6517.
31 M. S. Gudiksen, J. Wang and C. M. Lieber, *J. Phys. Chem. B*, 2002, **106**, 4036–4039.
32 M. Fox, *Optical Properties of Solids*, Oxford University Press, 2001.
33 H. Zhou, X. M. Chen, G. H. Wu, F. Gao, N. Qin and D. H. Bao, *J. Am. Chem. Soc.*, 2010, **132**, 1790–1791.
34 Y. Q. Gao, Z. M. Huang, Y. Hou, J. Wu, Y. J. Ge and J. H. Chu, *Appl. Phys. Lett.*, 2009, **94**, 011106.
35 E. D. Palik, *Handbook of Optical Constants of Solid*, Academic, New York, 1985.
36 S. Adachi, *Phys. Rev. B*, 1987, **35**, 7454–7463; S. Adachi, *Phys. Rev. B*, 1988, **38**, 12345–12352.
37 D. A. G. Brüggeman, *Ann. Phys. (Leipzig)*, 1935, **24**, 636.
38 C. M. Herzinger, B. Johs, W. A. McGahan, J. A. Woollam and W. Paulson, *J. Appl. Phys.*, 1998, **83**, 3323–3336.
39 W. H. Press, S. A. Teukolsky, W. T. Vetterling and B. P. Flannery, *Numerical Recipes in C: The Art of Scientific Computing*, Cambridge University Press, Cambridge, MA, 1992.
40 D. J. Singh, S. S. A. Seo and H. N. Lee, *Phys. Rev. B: Condens. Matter Mater. Phys.*, 2010, **82**, 180103.
41 P. D. Mitev, K. Hermansson, B. Montanari and K. Refson, *Phys. Rev. B: Condens. Matter Mater. Phys.*, 2010, **81**, 134303.
42 S. Y. Yang, J. Seidel, S. J. Byrnes, P. Shafer, C. H. Yang, M. D. Rossell, P. Yu, Y. H. Chu, J. F. Scott, J. W. Ager, L. W. Martin and R. Ramesh, *Nat. Nanotechnol.*, 2010, **5**, 143–147.
43 G. He, L. D. Zhang, G. H. Li, M. Liu and X. J. Wang, *J. Phys. D: Appl. Phys.*, 2008, **41**, 045304.
44 S. Bouarab, A. Vega and M. A. Khan, *Phys. Rev. B: Condens. Matter*, 1996, **54**, 11271–11275.
45 F. Tran and P. Blaha, *Phys. Rev. Lett.*, 2009, **102**, 226401.
46 A. D. Becke and E. R. Johnson, *J. Chem. Phys.*, 2006, **124**, 221101.
47 M. V. Schilfgaarde, T. Kotani and S. Faleev, *Phys. Rev. Lett.*, 2006, **96**, 226402.
48 M. Q. Cai, Z. Yin, M. S. Zhang and Y. Z. Li, *Chem. Phys. Lett.*, 2005, **401**, 405–409.